ARCHIVES OF MECHANICS
Arch. Mech. **73** (2), 175–200, 2021, DOI: 10.24423/aom.3610

# Numerical study on two dimensional distribution of streamwise velocity in open channel turbulent flows with secondary current effect

S. MOHAN[1)], S. KUNDU[2)], K. GHOSHAL[1)], J. KUMAR[1)]

[1)] *Department of Mathematics, IIT Kharagpur, Kharagpur-721302, India, e-mails: shivmohan58@gmail.com koeli@maths.iitkgp.ac.in, jkumar@maths.iitkgp.ac.in*

[2)] *Department of Mathematics, NIT Jamshedpur, Jharkhand-831014, India, e-mail: snehasis.math@nitjsr.ac.in*

For studying mechanism of sediment transport in river flows, open channel flow is a prototype. Flow has always three components of velocity for all types of channel geometry and for a time independent uniform flow along streamwise or main flow direction, all the components of velocity are functions of lateral and vertical coordinates. The present study investigates the two dimensional distribution of streamwise (or longitudinal) velocity starting from the Reynolds averaged Navier–Stokes equation for a turbulent open channel flow which is steady and uniform along the main flow direction. Secondary flows both along the vertically upward direction and along the lateral direction are considered which are also taken as functions of lateral and vertical coordinates. Inclusion of the secondary current brings the effect of dip phenomenon in the model. The resulting second order partial differential equation is solved numerically. The model is validated for all the cross-sectional, transverse and centreline velocity distribution by comparing with existing relevant set of experimental data and also with an existing model. Comparison results show good agreement with data as well as with the previous model proving the efficiency of the model. It is found that the transverse velocity distribution depends on the formation of circular vortex in the cross-sectional plane and becomes periodic as the number of circular vortex increases for increasing aspect ratios.

**Key words:** velocity distribution, open channel flow, turbulent flow, RANS equations, secondary current, Finite Difference Method.



## 1. Introduction

In the study of river hydraulics or any fluvial system, understanding the turbulent velocity distribution is one of the key components. Researchers worked since decades to develop different models on velocity distribution in an open channel flow considering different aspects of turbulence. But the fluctuating

behavior of turbulence is so unforeseeable that it never allowed any model to be universally acceptable. So the research on velocity in an open channel turbulent flow can never come to an end.

Usually in open channel turbulent flows, velocity distribution means the vertical distribution of streamwise time averaged velocity of the flow in the central section of an open channel where the side-wall effects are negligible. Pioneer in this field were VON KARMAN [1] and PRANDTL [2] whose law of wall is till now applied in the study of turbulence. After that, numerous models have been developed by several researchers [3–12] incorporating different features of turbulence in their models. All these models mainly focussed into one dimensional distribution of longitudinal velocity. One of the important aspects of turbulence is secondary current which is present in all kinds of flow irrespective of the channel geometry [13] and it helps to understand the flow as well as the variation of bed texture and bed topography. Several researches can be found in literature that studied structure and mechanism of secondary flow in an open channel. WANG and CHENG [14] investigated experimentally as well as analytically, the time-mean characteristics of cellular secondary flow that is generated by longitudinal bedforms. According to PRANDTL [2], two categories of secondary current can be identified in fluid flow. The first kind or skew-induced streamwise vortcity is originated from the mean flow and commonly treated by the researchers. The second kind secondary current is generated by turbulence which is related to the formation of sand ridges and is typical in straight and non-circular channels [15]. YANG *et al.* [16] studied in details the mechanism for initiation and retention of Prandtl's second kind secondary current. They revealed that secondary currents originate from the boundary region and the lateral variation of streamwise velocity is the cause of generation. Recently DUDA *et al.* [17] have experimentally observed the second kind secondary flow in a corner of a channel of the square cross-section by using Stereo Particle Image Velocimetry. They studied the generation and pattern of vortices for different Reynolds numbers. For narrow open channels where the aspect ratio (ratio of channel width to flow depth) is less then 5 [18], the influence of secondary current is prominent that brings the maximum streamwise velocity below the free surface, a phenomenon which is commonly known as the dip-phenomenon. The dip-phenomenon was reported quite a long time ago for open channels and rivers [19–21] as well as for laboratory tests [22, 23]. GUO and JULIEN [10, 24] and ABSI [11] developed a number of velocity models which are able to predict a dip-phenomenon. KUNDU and GHOSHAL [12] developed a modified velocity model known as the total-dip-modified-log-wake law which was fully analytical. GUO [25] revisited smooth rectangular open channel flow in terms of the velocity dip-position, the centreline and the cross-sectional velocity distributions. He derived the dip position by Yang's linear shear stress distribution and showed that centreline velocity

distribution and cross-sectional velocity distribution can be described by GUO and JULIEN's MLW law [10, 26].

All the above mentioned models mostly focussed on one dimensional distribution of longitudinal velocity in comparison to which two dimensional velocity distribution studies are quite less. SARMA *et. al.* [4] developed a two dimensional distribution formula for longitudinal velocity but the formula was not able to address the dip-phenomenon. LU [27] derived two dimensional velocity (longitidinal) expression for a steady uniform flow through open channels which was applicable in Yangtze river though the expression needed modification for application to rivers with narrow-deep cross-sections. BONAKDARI *et. al.* [28] proposed vertical shear stress distribution along a centreline considering secondary current effects and from that, developed an analytical solution for velocity with parabolic eddy viscosity. GUO [25] developed modified log wake law for cross-sectional velocity distribution empirically. Though the model of GUO [25] shows a dip effect, but effects of transverse and vertical components of velocity are not included in this model. He compared his model for centerline velocity distribution with the data of COLEMAN [6], LYN [29] and MUSTE and PATEL [30] and for cross-sectional velocity distribution, with the data of TOMINAGA *et. al.* [31] who measured the three dimensional turbulent structure in straight open channels including both primary velocity and secondary current. Recently, LU *et. al.* [32] have derived the longitudinal velocity distribution formula analytically along vertical and transverse directions with the sidewall effects starting from the Reynolds equation of a turbulent flow and validated their model with both laboratory and channel data. Though the agreement was satisfactory, but they excluded some terms (explained later) in the governing equation without any proper explanation.

From the aforementioned literature review it can be observed that previous studies mostly were associated with one dimensional distribution of the streamwise velocity component that depends on the vertical coordinate only. Very few researchers studied two dimensional distribution of streamwise velocity, but either not including influence of secondary current resulting into dip-phenomenon or not taking into account the transverse and vertical components of velocity or neglecting some relevant terms from the governing equation. Literature lacks in a generalized model that originates from traditional mass and momentum equations and studies the streamwise velocity considering velocity components in all three directions that are functions of lateral and vertical coordinates. So the present study devotes to develop a model starting from the Reynolds averaged Navier–Stokes (RANS) equation for streamwise velocity for a steady and uniform flow along the main flow direction and which includes the effect of both transverse and vertical velocities resulting into a solution containing the dip-phenomenon, all the velocity components being functions of lateral and vertical

coordinates. This work can be considered as an extension of LU *et al.* [32] work who started from RANS equation, but not considering few important terms, may be for the sake of providing an analytical solution. The present work considers those terms and provides a numerical solution to the problem.

In brief, the main objectives of the present study are (i) to investigate the two dimensional longitudinal velocity distribution in a steady turbulent flow uniform along the main flow direction, through straight open channels starting from RANS equation with all three velocity components; (ii) to apply a numerical method for solving the partial differential equation arising in such flows; (iii) to validate the obtained solution with relevant experimental data containing the dip phenomenon; and (iv) to demonstrate the solution with other existing model to investigate transverse velocity distributions.

## 2. Derivation of the 2D velocity distribution model

We consider a steady, uniform (along longitudinal direction) turbulent flow through a straight rectangular open channel with the width $2B$ and the energy slope $S$. In the three dimensional cartesian co-ordinate system, $x$, $y$ and $z$ indicate the main flow, lateral and vertical directions respectively as shown in Fig. 1 and

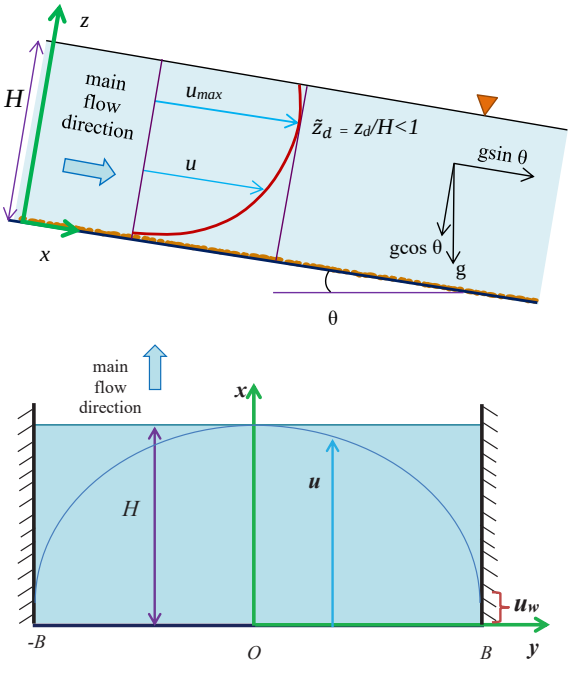


FIG. 1. Schematic diagram of the two dimensional velocity distributions along vertical ($z$) (figure in the top) and transverse ($y$) (figure in the bottom) directions.

the origin $O$ is considered at the bottom of the center line. Let $u(y,z)$, $v(y,z)$ and $w(y,z)$ denote the mean flow velocities along streamwise (or longitudinal), lateral (or transverse) and vertical directions respectively. Then the mass conservation and $x$-directional momentum equations are expressed after taking the Reynolds averaging (RANS equation) as

$$\frac{\partial v}{\partial y}+\frac{\partial w}{\partial z}=0, \tag{2.1}$$

$$\frac{\partial u}{\partial y}+w\frac{\partial u}{\partial z}=g_x+\nu\left(\frac{\partial^2 u}{\partial y^2}+\frac{\partial^2 u}{\partial z^2}\right)+\left[\frac{\partial}{\partial y}(-\overline{u'v'})+\frac{\partial}{\partial z}(-\overline{u'w'})\right], \tag{2.2}$$

where $g_x = g\sin\theta = gS$ (say) denotes the component of a gravitational force along the main flow direction, $\theta$ is the channel slope, $\nu$ denotes fluid kinematic viscosity, $u'$, $v'$ and $w'$ denote turbulent fluctuating components of corresponding velocities and overbars denote the time averaging. Equation (2.2) can be further expressed as

$$v\frac{\partial u}{\partial y}+w\frac{\partial u}{\partial z}=gS+\frac{1}{\rho}\frac{\partial}{\partial y}(\tau_{xy}^{\mathrm{tot}})+\frac{1}{\rho}\frac{\partial}{\partial z}(\tau_{xz}^{\mathrm{tot}}), \tag{2.3}$$

where $\rho$ is fluid density, $\tau_{xy}^{\mathrm{tot}}$ and $\tau_{xz}^{\mathrm{tot}}$ are components of total shear stresses which are expressed as follows

$$\tau_{xy}^{\mathrm{tot}}=\mu\frac{\partial u}{\partial y}+(-\rho\overline{u'v'})=\tau_{xy}^{\nu}+\tau_{xy} \tag{2.4}$$

and

$$\tau_{xz}^{\mathrm{tot}}=\mu\frac{\partial u}{\partial z}+(-\rho\overline{u'w'})=\tau_{xz}^{\nu}+\tau_{xz}. \tag{2.5}$$

Here $\tau_{xy}^{\nu}$ and $\tau_{xy}^{\nu}$ are viscous shear stresses and $\tau_{xy}$ and $\tau_{xz}$ are Reynolds shear stresses. In open-channel flows, viscous shear stresses are dominant in the thin viscous sublayer and above this layer, in the main flow region, Reynolds shear stresses dominate. Therefore Eqs. (2.4) and (2.5) are approximated by ignoring the viscous terms and then using the Boussinesq hypothesis [3] and the uniform flow condition, we can write

$$\tau_{xy}^{\mathrm{tot}}\approx-\rho\overline{u'v'}=\tau_{xy}=\rho\nu_y\left(\frac{\partial u}{\partial y}+\frac{\partial v}{\partial x}\right)=\rho\nu_y\frac{\partial u}{\partial y} \tag{2.6}$$

and

$$\tau_{xz}^{\mathrm{tot}}\approx-\rho\overline{u'w'}=\tau_{xz}=\rho\nu_z\left(\frac{\partial u}{\partial z}+\frac{\partial w}{\partial x}\right)=\rho\nu_z\frac{\partial u}{\partial z}, \tag{2.7}$$

where $\nu_y$ and $\nu_z$ are eddy viscosities along lateral and vertical directions respectively. Substituting Eqs. (2.6) and (2.7) into Eq. (2.3), the governing equation for 2D flow is expressed as

$$\frac{\partial}{\partial y}\left(\nu_y \frac{\partial u}{\partial y}\right) + \frac{\partial}{\partial z}\left(\nu_z \frac{\partial u}{\partial z}\right) - v\frac{\partial u}{\partial y} - w\frac{\partial u}{\partial z} = -gS. \tag{2.8}$$

Secondary current of Prandtl's second kind is generated by the non-uniformities of the flow near the walls induced by the anisotropic turbulence [33]. These secondary currents of the second kind are weak and have magnitude of the maximum velocity less than 5% of the mean streamwise flow velocity [34]. PRANDTL [35] postulated that the distribution of longitudinal mean velocity in a cross-sectional plane changes due to the presence of secondary flows. Therefore the flow with effects of secondary current can be assumed as a flow with the primary flow superimposed with the weak secondary flow and is a result of perturbation to the primary flow due to the existence of secondary currents [36]. As a result LU *et. al.* [32] considered $v(y,z)/u(y,z)$ and $w(y,z)/u(y,z)$ to be of small order and neglected the last two product terms in the LHS of Eq. (2.8) assuming linear stability. But since the cross-sectional distribution of primary mean flow velocity is subjected to change with the presence and structure of secondary velocities $v$ and $w$ [14], these terms must be taken into account and therefore in this study we consider Eq. (2.8) as the governing equation for 2D velocity distribution.

The eddy viscosity $\nu_z$ along vertical direction is modeled by the parabolic profile after assuming the linear law of fluid shear stress and the logarithmic law of streamwise mean velocity $u$ as [37, 38]

$$\nu_z = \kappa u_{*b} z\left(1 - \frac{z}{H}\right), \tag{2.9}$$

where $\kappa$ is the von Karman coefficient, $u_{*b} = \sqrt{\tau_b/\rho}$ is the local bed shear velocity i.e. the shear velocity along lateral/transverse direction in which $\tau_b$ is the bed shear stress and $H$ is the flow depth. TOMINAGA *et al.* [31] experimentally showed that in narrow open channels, free surface and bottom vortices/eddies exist and they transfer low momentum water from side walls to the central section of open channels that causes the dip-phenomena. Later YANG *et al.* [9] and GUO [25] modeled the secondary current effect in the Reynolds shear stress distribution using the combination of two shear stresses $\tau_b$ and $\tau_1$ where $\tau_1$ is the 'apparent' shear stress at the free surface. It acts like a shear stress but it signifies the momentum transfer by secondary current near the free surface only. GUO [25] showed after analyzing data of TOMINAGA *et al.* [31] that dip-phenomenon occurs due to the presence of longitudinal water surface eddies which increase the maximum velocity through the wake function and for narrow open channels, the

wake function [3] is scaled by another shear velocity $u_{*1}$ as proposed by GUO [25] and along the center line, the modified log-wake (MLW)-law is finally scaled by $u_{*b} + u_{*1}$ [25]. Since the distribution of mean streamwise velocity also changes with lateral direction, $u_{*b} + u_{*1}$ cannot be used for scaling the velocity $u(y, z)$. WANG and CHENG [36] suggested that if $\widetilde{u}_*(= \sqrt{ghS})$ denotes the average shear velocity at the central section, then at different sections of channel, $u_{*b}$ changes along the lateral direction as

$$\frac{u_{*b}}{\widetilde{u}_*} = \left[1 + 0.18\cos\left(\frac{\pi y}{H}\right)\right]^{1/2}. \tag{2.10}$$

Here it can be observed from Eq. (2.10) that the change of $u_{*b}$ along lateral direction is due to the presence of the cosine term on the right side of this equation and therefore the spatially averaged shear velocity $\overline{u}_*$ along the transverse direction can be defined as [36]

$$\begin{aligned}\overline{u}_* &= \frac{1}{2B}\int_{-B}^{B} \widetilde{u}_*\left[1 + 0.18\cos\left(\frac{\pi y}{H}\right)\right]^{1/2} dy \\ &= \frac{\widetilde{u}_*}{Ar/2}\int_{0}^{Ar/2} [1 + 0.18\cos(\pi t)]^{1/2}\, dt,\end{aligned} \tag{2.11}$$

where $Ar = \frac{2B}{H}$ is the aspect ratio. Since $\overline{u}_*$ gives the average value, therefore it is more reasonable to use $\overline{u}_*$ for scaling the velocity components. Therefore using Eq. (2.11), the eddy viscosity along the vertical direction is expressed as

$$\nu_z = \kappa\lambda\overline{u}_* z\left(1 - \frac{z}{H}\right), \tag{2.12}$$

where $\lambda = Ar/[2\int_0^{Ar/2}[1 + 0.18\cos(\pi t)]^{1/2}\, dt]$ is a constant. It is to be noted that when bed effects are absent, the integrand on the right side of Eq. (2.11), is simply 1 and one gets $\overline{u}_* = \widetilde{u}_* = \sqrt{ghS}$.

As such no general empirical model exists in literature for the eddy viscosity model along the lateral direction. It is general practice in river engineering to approximate it by its average value and such a model was proposed by IKEDA [39]. Following [18, 39], in the absence of bed roughness or bed elevation, $\nu_y$ along the lateral direction is approximated by the depth-averaged eddy viscosity as

$$\nu_y = \frac{\kappa}{6}\overline{u}_* H, \tag{2.13}$$

where $\overline{u}_*$ is the spatially averaged shear velocity in the transverse direction which is already defined.

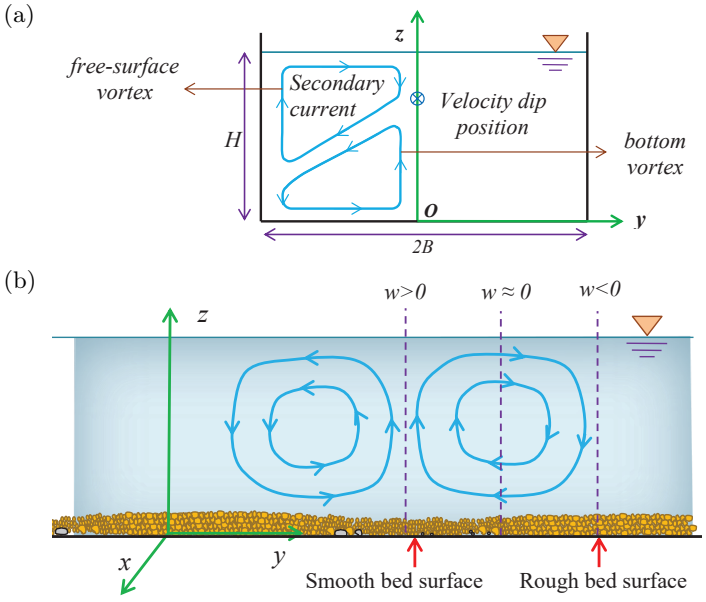


FIG. 2. Schematic pattern of secondary current. (a) In narrow open channel according to [44]; (b) In wide open channel with alternate smooth and rough bed strips [45].

The structure of secondary currents occuring in narrow and wide open channels are different (see Fig. 2). In narrow open channels, due to the sidewall effects, free surface vortex and bottom vortex are generated and for wide open channels, free surface vortex gradually disappears. The dip-phenomenon occurs due to the presence of the free surface vortex [25]. In the free surface vortex, the secondary flow velocity $w(y,z)$ is acting along the vertically downward direction at the centerline and along vertically upward direction near the sidewall. Therefore such flow velocity can be modeled from [14] as

$$w(y,z) = -w_{max}\sin\left(\pi\frac{z}{H}\right)\cos\left(\pi\frac{y}{H}\right), \tag{2.14}$$

where $w_{max}$ is the maximum flow velocity of $w$. Substituting Eq. (2.14) into Eq. (2.1) and integrating, the lateral secondary flow velocity is obtained as [14]

$$v(y,z) = w_{max}\cos\left(\pi\frac{z}{H}\right)\sin\left(\pi\frac{y}{H}\right). \tag{2.15}$$

Finally, substituting Eq. (2.13) and Eqs. (2.12)–(2.15) into Eq. (2.8) and using the following dimensionless variables

$$\widetilde{z} = \frac{z}{H}, \quad \widetilde{y} = \frac{y}{H}, \quad \widetilde{u} = \frac{u}{\overline{u}_*}, \quad \widetilde{v} = \frac{v}{\overline{u}_*} \quad \text{and} \quad \widetilde{w} = \frac{w}{\overline{u}_*} \tag{2.16}$$

the governing equation is rewritten as

$$\frac{\partial^2\widetilde{u}}{\partial\widetilde{y}^2}+6\lambda\widetilde{z}(1-\widetilde{z})\frac{\partial^2\widetilde{u}}{\partial\widetilde{z}^2}-\left(\frac{6}{\kappa}\right)\widetilde{v}\frac{\partial\widetilde{u}}{\partial\widetilde{y}}+\left[6\lambda(1-2\widetilde{z})-\left(\frac{6}{\kappa}\right)\widetilde{w}\right]\frac{\partial\widetilde{u}}{\partial\widetilde{z}}+\frac{6gSH}{\kappa\overline{u}_*^2}=0. \tag{2.17}$$

The distribution of primary mean flow velocity $\widetilde{u}(\widetilde{y},\widetilde{z})$ in the yz cross-sectional plane is governed by Eq. (2.17). Here secondary velocities $\widetilde{v}$ and $\widetilde{w}$ are given in Eqs. (2.14) and (2.15), respectively. It can be observed that the governing equation is an elliptic partial differential equation. To find the solution of Eq. (2.17), apart from boundary conditions, some more conditions are required which are conditions at dip position, at centerline and at a wall. All the conditions can be written together as

$$\widetilde{u}(\widetilde{y},\widetilde{z})\big|_{\widetilde{z}=0}=\widetilde{u}_a,\quad \widetilde{u}(\widetilde{y},\widetilde{z})\big|_{\widetilde{z}=1}=\widetilde{u}_s, \tag{2.18}$$

$$\frac{\partial\widetilde{u}}{\partial\widetilde{z}}\big|_{\widetilde{z}=\widetilde{z}_d}=0, \tag{2.19}$$

$$\frac{\partial\widetilde{u}}{\partial\widetilde{y}}\big|_{\widetilde{y}=0}=0, \tag{2.20}$$

and

$$\widetilde{u}(\widetilde{y},\widetilde{z})\big|_{\widetilde{y}=|B/H|}=\widetilde{u}_w, \tag{2.21}$$

where $\widetilde{u}_a(=u_a/\overline{u}_*)$ denotes the primary mean flow velocity at bottom (it is generally taken as zero or very small), $\widetilde{u}_s(=u_s/\overline{u}_*)$, denotes the primary mean flow velocity at free surface, $\widetilde{z}_d=z_d/H$ is the dimensionless height of velocity dip-position from channel bed, $\widetilde{u}_w=u_w/\overline{u}_*$ is the mean sidewall flow velocity. In Eq. (2.21), modulus sign is given to indicate the both sidewall positions from centreline. Equation (2.17) along with the conditions Eqs. (2.18)–(2.21) is solved numerically using the finite difference approximation. As this method is well established and is quite often used to solve ordinary/partial differential equation, it is not described in the main text of the manuscript. It has been given in the appendix for those readers who are not familiar with this method.

## 3. Validation of the model

In this section, we have validated our obtained numerical solution using the finite difference numerical scheme with the existing analytical and numerical solutions as well as experimental data under some specific conditions. To obtain the numerical solution of a problem, discretization of computational domain is an important aspect as the accuracy of the numerical solution depends on the grid size. The best way to obtain the grid converged solution is by plotting the

solution with more and more number of grid sizes until one finds that there is no significant difference in the solutions. For that purpose, in the present work, the computational domain is divided into $N$ number of equally spaced grid points with the grid size $\Delta\tilde{y} = \frac{L_y}{N-1}$ in $\tilde{y}$-direction and $M$ number of equally spaced grid points with the grid size $\Delta\tilde{z} = \frac{L_z}{M-1}$ in $\tilde{z}$-direction. $L_y$ and $L_z$ are the lengths of the domain in $\tilde{y}$ and $\tilde{z}$ directions, respectively. More detailed explanation is given in appendix.

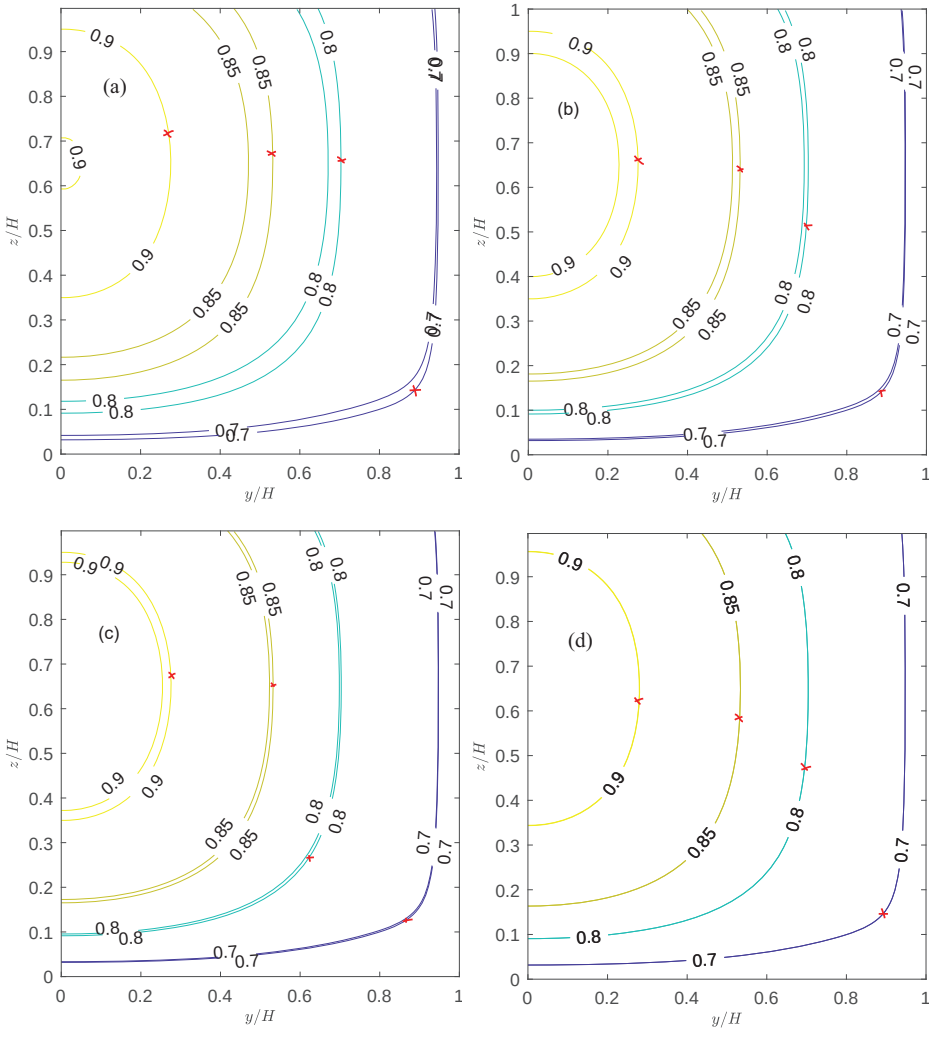


FIG. 3. Sensitivity of cross-sectional velocity distribution for different grid size (a) $M = N = 90$, (b) $M = N = 110$, (c) $M = N = 140$ and (d) $M = N = 180$. The contour lines with cross symbol show the benchmark solution corresponding to 200 grid points each for $M$ and $N$.

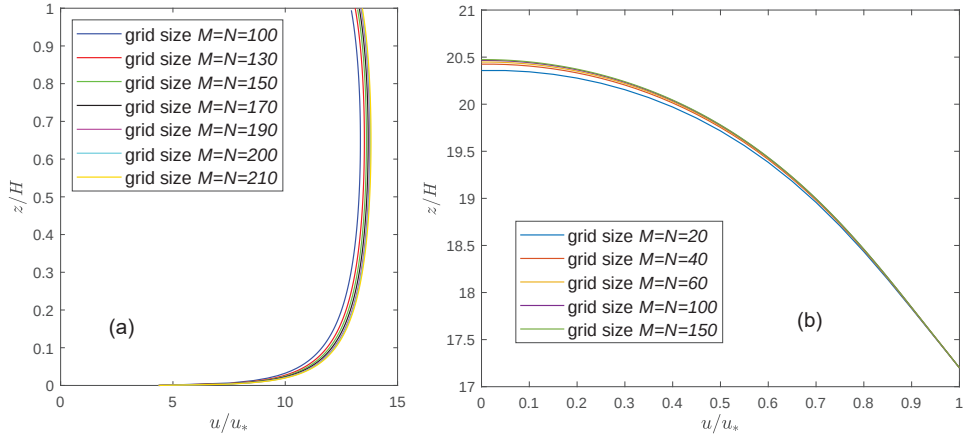


FIG. 4. Sensitivity of vertical and transverse velocity distributions with different grid sizes (a) vertical, (b) transverse.

To obtain the converged solution over different grid sizes, we have plotted cross-sectional, vertical and transverse velocity profiles in Figs. 3 and 4 respectively for different number of grid points. In case of the cross-sectional velocity, we have considered different grids sized in both the directions. In Fig. 3, the cross-sectional solutions are plotted for four different choices of grid sizes. From the plots in Fig. 3, it can be observed that if one considers grid points greater than 180 in both directions, the grid converged solution is obtained. Here, the solution with 200 grid points in both directions is considered as the benchmark solution and plotted together with other grid point solutions in Fig. 3 to show the convergence. It is found that after a minimum number grid point of 180 in both directions, the solution becomes less sensitive and does not increase significantly. Similarly in Fig. 4, the vertical and transverse variations with different grid sizes are plotted. From the figures it can be observed that after 200 grid points vertical velocity converges and after 120 grid points the transverse velocity converges. This analysis shows the stability of the numerical solutions.

### 3.1. Cross-sectional velocity distribution

To test the validity of the proposed numerical solution of Eq. (2.17), experimental data of TOMINAGA *et. al.* [31] has been used. They measured the 3D turbulent structure with hot-film anemometers in three straight open channels, including a rectangular flume 12.5 m long and 40 cm × 40 cm cross-section. The bed-wall was made with an iron plate and painted for smoothness and a sidewall was made up with glass materials. The fully developed, uniform turbulent flow

was established at the test section 7.5 m downstream from the entrance of a channel by adjusting the bed slope and the movable weir at the channel end. In this group of experiments, the channel width $2B$ was kept fixed and the flow depth $H$ was changed. Three flow depth cases were considered with depths $H = 5$ cm, 10.15 cm and 19.90 cm. In this experiment, the maximum value of secondary current is about 1.5% of the maximum value of the streamwise mean flow velocity $u_{max}$. The results include the measured data for the primary mean flow velocity, secondary currents and turbulence intensities. Other experimental conditions are given in Table 1. In Fig. 5, primary mean velocity distribution along the $yz$ cross-sectional plane is plotted corresponding to three different cases. In the left column of the figure, the cross-sectional mean velocity for the left half cross-section is plotted from the experimental data of Tominaga et. al. [31] and the calculated cross-sectional mean velocity from the numerical solution for the right half cross-section are plotted in the right column. In the computed solution, the value of the local bed shear velocity $u_{*b}$ is calculated from Eq. (2.10) and values of other parameters are taken from experiments of [31]. It can be observed from Fig. 5 that the proposed solution provides good agreement with the experimental measurements.

**Table 1. Experimental conditions and values of parameters for experiment of [31].**

| Cases | Flow depth $H$ [cm] | Aspect ratio $Ar$ | Bed shear velocity $u_{*b}$ [cm/s] | Maximum velocity $u_{max}$ [cm/s] | $\widetilde{u}_a$ [cm/s] | $\widetilde{u}_w$ [cm/s] |
|---|---|---|---|---|---|---|
| S1 | 5.00 | 8.00 | 2.14 | 46.31 | 5.96 | 14.16 |
| S2 | 10.15 | 3.94 | 1.17 | 23.50 | 8.07 | 11.96 |
| S3 | 19.90 | 2.01 | 1.64 | 24.36 | 4.36 | 9.96 |

### 3.2. Transverse velocity distribution

Similarly, the validity of the numerical solution of Eq. (2.17) to predict the velocity distribution along the transverse direction at different vertical heights is also tested. Experimental data of SARMA *et. al.* [4] for rectangular open channel is considered here. In [4] they studied the velocity distribution in rectangular open channels dividing the cross-sectional region into four parts. The experiments were conducted in a straight, horizontal rectangular flume of smooth walls with length 15.25 m, width 61 cm, and height 30 cm. The experiments were conducted in two stages. The first stage of experiments were carried out in 61 cm wide flume and in the second phase, experiments were carried out in a 30.5 cm wide flume covering the range of the aspect ratio $Ar$ from 1 to 8 in both the stages. The channel bed was kept very nearly horizontal. They assumed a parabolic type profile for region 1 which is the inner region of bed and outer

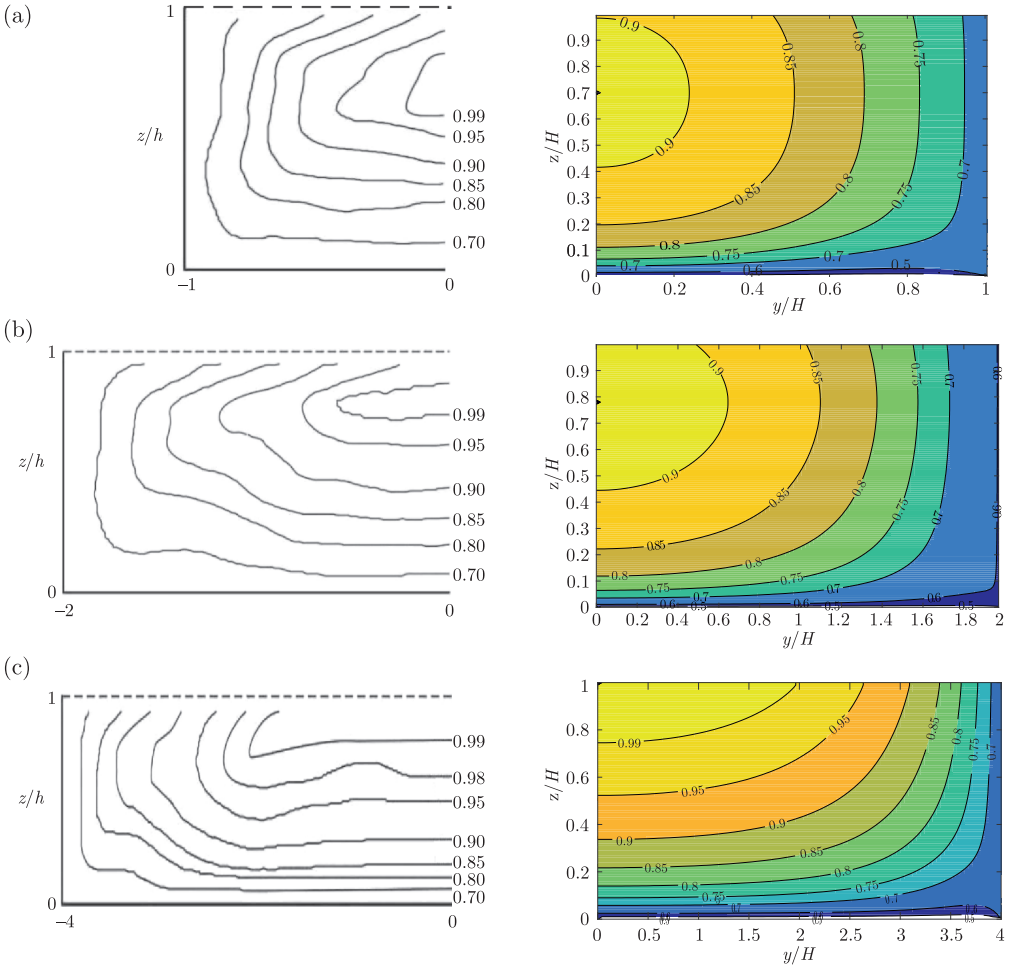


FIG. 5. Comparison of computed velocity contours from numerical solution (in right column) with the experimental data from [31] (in left column) as $u/u_{max}$ for (a) Case S3, $Ar = 2.01$, (b) Case S2, $Ar = 4$ and (a) Case S1, $Ar = 8$.

region of sidewall. The parabolic profile assumed by them can be put as

$$\frac{u_{max} - u}{\overline{u}_*} = K_w \left(1 - \frac{y}{B}\right)^2, \tag{3.1}$$

where $K_w$ is the coefficient in the law for the outer region of the sidewall very close to the bed obtained as 2.4, $B$ is the width of half channel. Figure 6 shows the validity of the proposed model in predicting the transverse velocity distribution with the experimental data of [4] for the aspect ratios $Ar = 2$ and 8 for narrow and wide open channels, respectively. The model [4] i.e. Eq. (3.1) is also plotted

in the figure to compare with the proposed model. In Fig. 6a, the dimensionless transverse velocity $u/u_*$ is plotted as a function of $y/H$ for the aspect ratio 2 and $z/H = 0.1$. The values of parameters are taken as $\widetilde{u}_a = 22$, $\widetilde{u}_w = 5.7$, $B = 15.25$ cm, $\widetilde{u}_{max} = 22.9$ m/s, $\widetilde{z}_d = 0.59$. The parameters are crucial for accurately predicting the position of the velocity dip and needs appropriate calculation; [40] compared all available models of dip-position in literature and proposed a new model using the concept of entropy theory. For the comparison analysis in this study, the model of [40] is chosen as it gives accurate prediction and minimum errors. The formula is expressed as

$$\widetilde{z}_d = 0.5 + \frac{1}{2L}\ln[1 + (e^L - 1)\{1 - e^{-0.07Ar^{1.18}}\}], \tag{3.2}$$

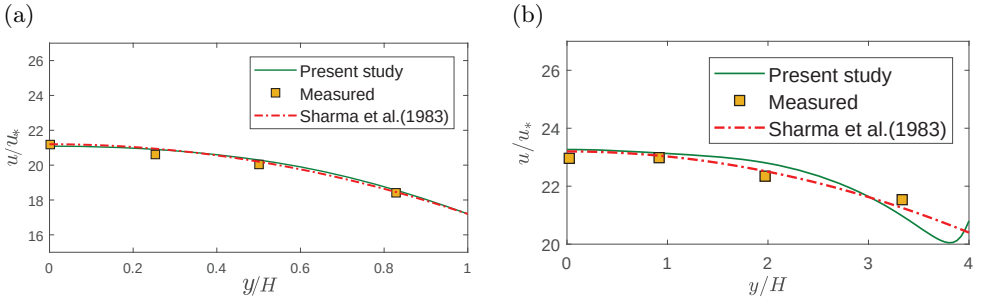


FIG. 6. Comparison of calculated transverse velocity distribution in rectangular open channel with the experimental data and model of [4]: (a) $Ar = 2$; (b) $Ar = 8$.

where $L = 0.724$. Similarly, in Fig. 6b, the dimensionless transverse velocity $u/u_*$ is plotted as a function of $y/H$ for the aspect ratio 8 and $z/H = 0.04$. The values of parameters are taken as $\widetilde{u}_a = 23.2$, $\widetilde{u}_w = 0.7$, $B = 30.5$ cm, $\widetilde{u}_{max} = 22.9$ m/s, $\widetilde{z}_d = 1$. From the figures it can be observed that the proposed model can predict the transverse velocity distribution at different vertical heights for both narrow and wide rectangular open channels. Also that in case of a narrow channel, both the models give good agreement through out the channel cross-section; whereas for a wide open channel, present study slightly deviates from both the experimental data and the empirical model of [4] near the vertical side-wall. This deviation can be explained as follows: in natural channels or wide open channels, the flow structure is three dimensional. Therefore the existence and the structures of the cellular secondary velocities play significant role on the distribution of transverse velocities. Generally the second kind of cellular secondary current appears as counter rotating paired cells and occurs periodically along the transverse direction with an approximate period of twice the height/depth of the flow $H$ as shown in Fig. 2 [14, 16, 41]. In case of narrow

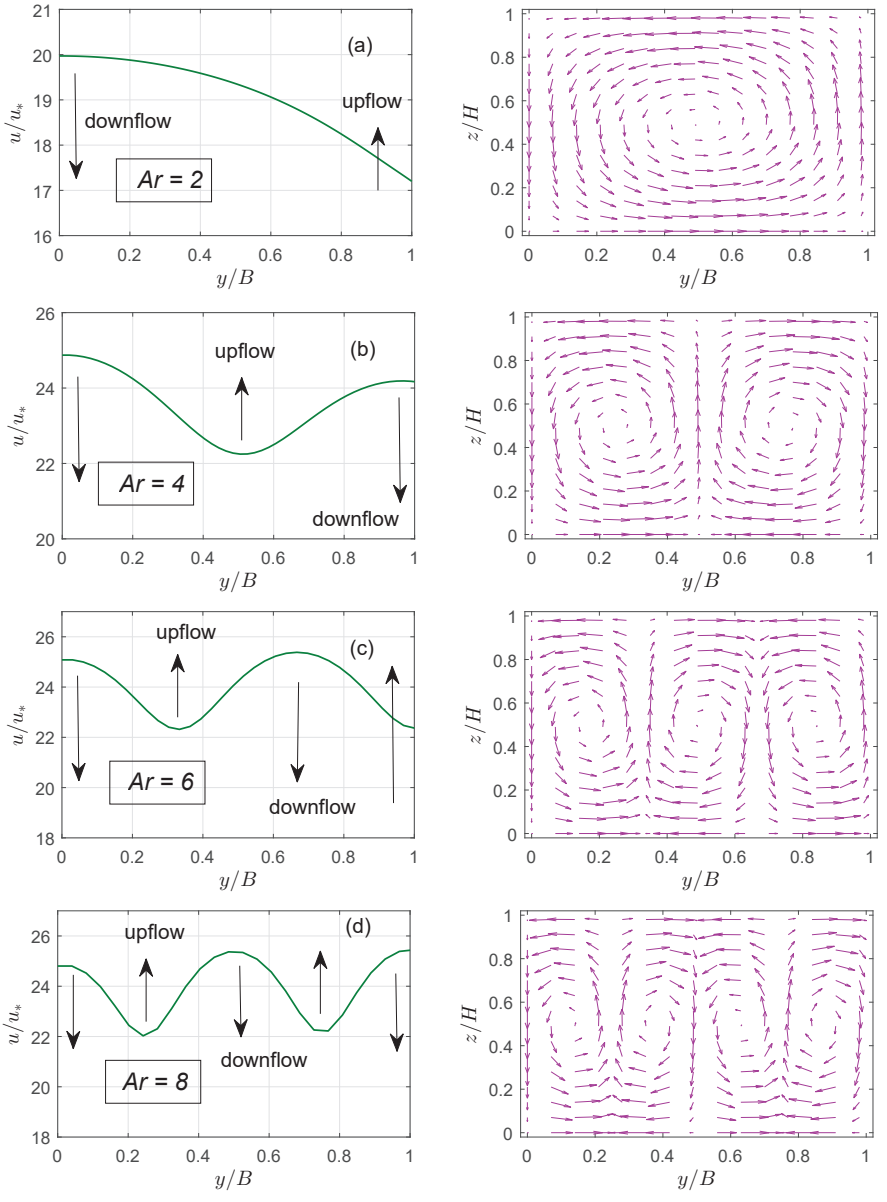


FIG. 7. Variation of transverse velocity with secondary circulations for different aspect ratios and alternate bottom surfaces. Left column represents the transverse velocity distribution and right column represents the circular secondary currents in half cross-sectional plane for different aspect ratios.

channels where $Ar = 2$ or $B = H$ only one pair of counter rotating circular cells exist and as a consequence, the periodicity does not occur. Therefore in Fig. 6a the proposed solution matches exactly. On the other hand, in case of a wide

open channel where $Ar = 8$ or $B = 4H$, four pairs of cellular secondary cells exist and the transverse velocity profile becomes periodic. In our present study we have included the existence of the circular secondary currents to make the model more appropriate and realistic by considering most appropriate models of secondary velocities proposed by [14] as trigonometric functions. As a consequence the numerical results slightly deviates from the experimental data near the wall boundary. In case of the model of [4], the deviation disappears as they considered only a parabolic type empirical model for transverse velocity distribution where a periodicity effect is not present. Apart from this, the result also deviates due to the existence of the corner bottom vortex near the side wall region.

To discuss the variation of primary velocity along the transverse direction and deviation of the proposed model near the vertical wall region Fig. 7 is plotted. In the figure, the transverse velocities are plotted in the left column and the cross-sectional velocity vectors from Eqs. (2.14) and (2.15) in the right column for four different choices of aspect ratios 2, 4, 6 and 8. The values of other parameters are taken from the experiments of [4] and $z/H = 0.1$. In all the plots of Fig. 7, the value of $y$ is taken from zero to half of the width $B$ of the channel. From the figure it can be observed that as an aspect ratio increases, the transverse velocity changes and behaves like a periodic function. From Fig. 7a, it can be seen that when the aspect ratio is 2, then $B = H$ and there exists only one circular vortex in the half cross-sectional plane (since the total width of pair of counter rotating circular vortex is $2B$). Apart from that, single upflow and downflow zones exist; and maximum and minimum transverse velocities correspond to downflow and upflow zones respectively. The result of $Ar = 2$ is consistent with the experimental observations of [4] and [14]. As the aspect ratio increases to 4, then $B = 2H$ and thus one pair of circular vortex occurs in the half cross-sectional plane as observed in Fig. 7 that corresponds to one upflow and two downflow zones. As a result, the transverse velocity attains one minimum and two maximum values. In a similar manner, with the increase of the aspect ratio the distribution of primary velocity along the transverse direction becomes periodic. These findings are new and are consistent with the experiments of [14].

### 3.3. Centreline velocity distribution

To find the velocity distribution along vertical direction at the center line, the value $\widetilde{y} = 0$ is taken. Experimental data of COLEMAN [5] has been used to validate the numerical solution at the central sections of narrow open channel flow. Coleman did experiments in a flume which was 356 mm wide and 15 m long. During the experiments, the energy slope $S$ was kept to be 0.002 except the last three test cases where $S$ was 0.0022. The flow depth was nearly constant and about 1.71 m. The temperature were in between 19.5 and 25.3°C. Among

40 test cases, test cases 1, 21 and 32 were performed in clear water flow and for validation of the model these runs have been considered. In all test cases / RUNS the aspect ratio is maintained as $Ar \approx 2$. The computed horizontal velocity from Eq. (2.17) is plotted in Fig. 8 and the values of the parameters are mentioned inside the figures. Here the bed velocity $\widetilde{u}_a$, $\overline{u}_*$ $(= u_*, \text{local shear velocity})$ and other values of parameters are considered from the experimental data. From the figure it can be seen that the proposed model can predict the vertical distribution of mean streamwise velocity well.

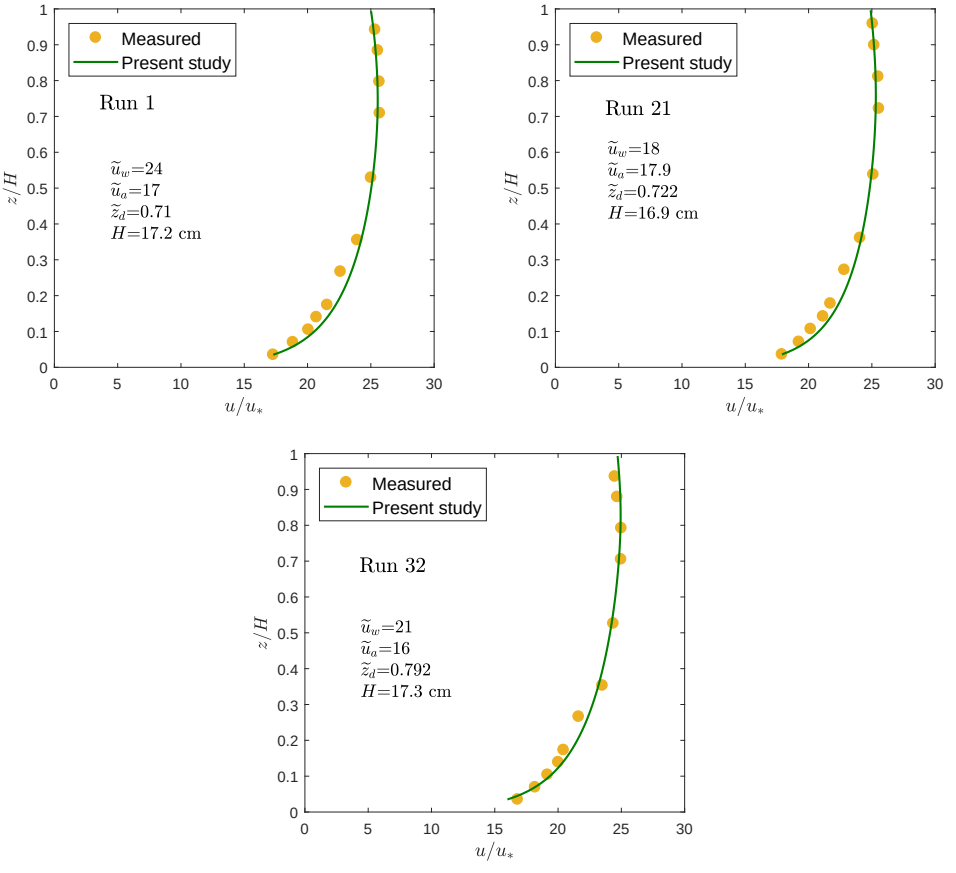


FIG. 8. Comparison of centreline velocity distribution with experimental data of COLEMAN [6].

Similarly, to test the velocity distribution along the vertical direction at the center line in a wide open channel, experimental data of VANONI [42] is considered. VANONI [42] performed experiments in two series. The experiments were done in a flume which is 0.8446 meter wide and 18.288 meter long with an ad-

justable bed slope. For validation purpose, test cases 1, 18 and 20 have been chosen. In all the test cases the aspect ratio varies from 5 to 11.90 and the maximum velocity appears at the free surface. The computed velocity from Eq. (5.17) is plotted in Fig. 9. Here also the values of parameters are given inside the figures. From the comparison results it can be concluded that the proposed model can predict the vertical velocity distribution in wide open channels well.

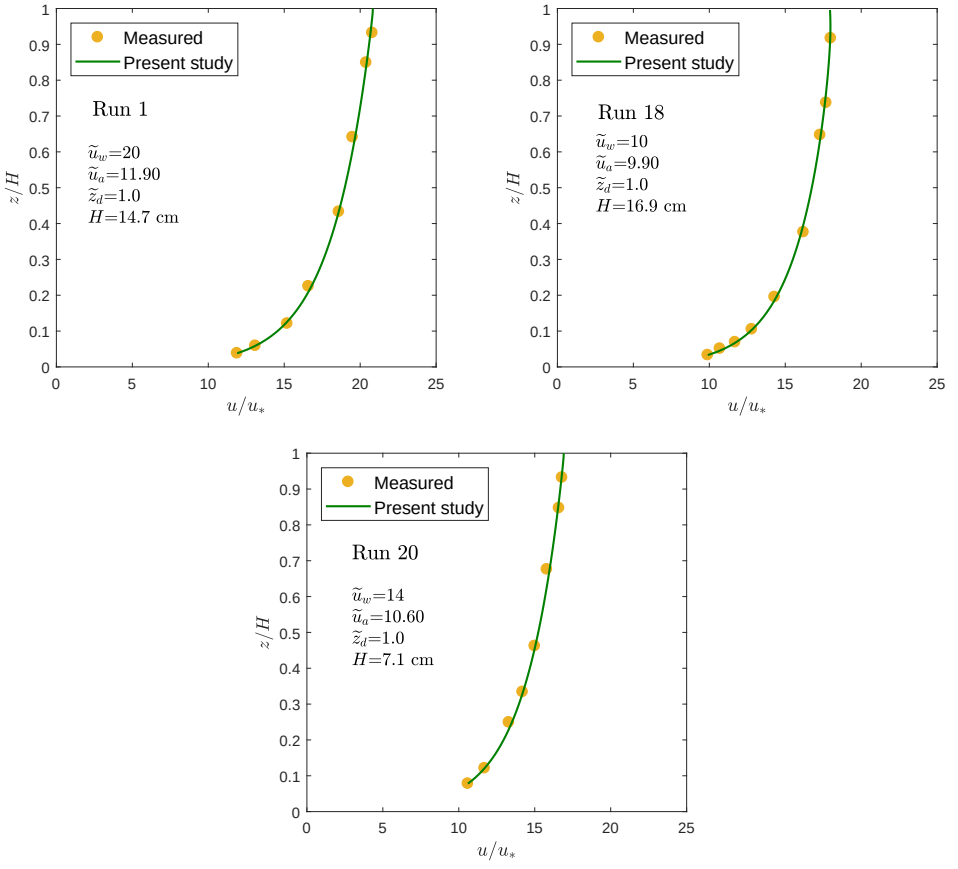


FIG. 9. Comparison of centreline velocity distribution with experimental data of VANONI [42].

Apart from the experimental data of COLEMAN [5] and VANONI [42], the present problem is also validated with the experimental data of WANG and QIAN [43] at the center line. WANG and QIAN [43] performed a series of experiments in a 30 cm wide, 40 cm high and 20 m long recirculating, tilting flume. For a vertical velocity profile, 4 clear water experiments, namely CW1, CW2, CW3 and CW4 were measured at center line. The computed velocity in the vertical direction is plotted in Fig. 10 with the experimental data of WANG

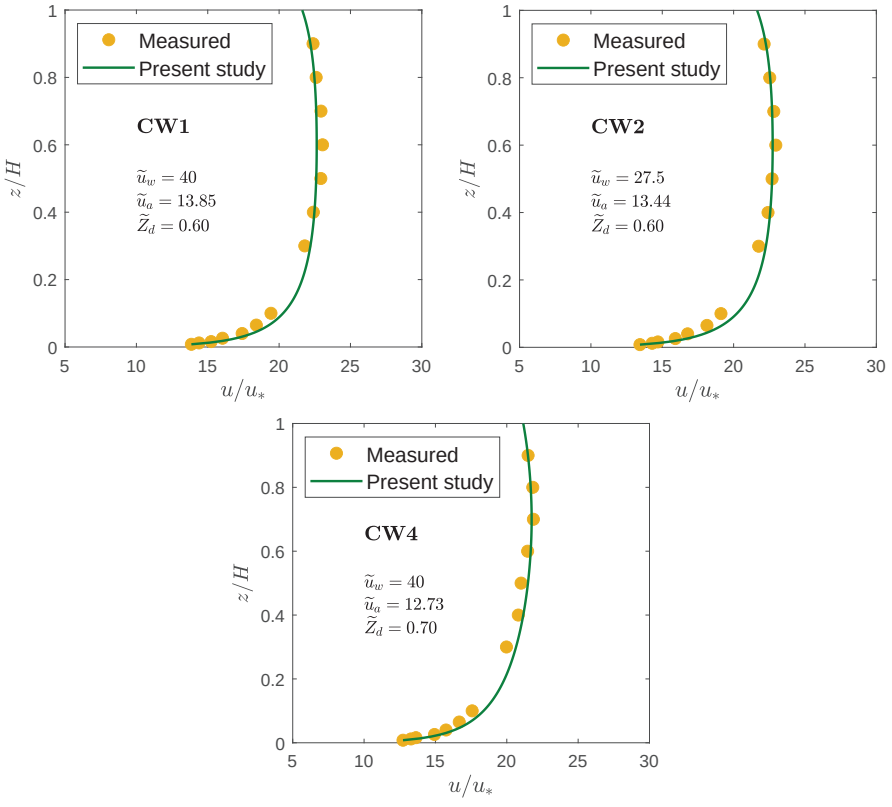


FIG. 10. Comparison of centreline velocity distribution with experimental data of WANG and QIAN [43].

and QIAN [43] for three data sets CW1, CW2 and CW4. The values of required parameters are mentioned within the figure. It is clear from Fig. 10 that the result agrees very well with the experimental data.

## 4. Conclusions

The following conclusions can be drawn from the present study:

(i) Starting from the $x$-component of the widely known Reynolds Averaged Navier Stokes (RANS) equation, the present study derives the two dimensional distribution of streamwise velocity in a turbulent flow in which the flow is considered steady and uniform along main (streamwise/longitudinal) direction. Different expressions for eddy viscosity for vertical and lateral (transverse) directions have been considered. Also secondary flow along these two directions has been taken into account where these are the functions of lateral and vertical coordinates.

(ii) The proposed model for streamwise velocity distribution that comes by solving a second order partial differential equation, is capable of describing the dip-phenomenon i.e. the occurrence of maximum velocity below the free surface which is mainly observed in narrow open channels.

(iii) From the proposed model, all the cross-sectional, transverse and centreline vertical velocity distributions have been compared with existing experimental data for validation purpose. Quite a good agreement is observed everywhere proving the justification of the model in determining two dimensional streamwise velocity in open channels.

(iv) It is established that when the aspect ratio increases, the proposed model gives good estimation of the transverse velocity and can also predict the periodic nature of it for wide open channels. Further it is found that for wide open channels with counter rotating circular secondary currents, transverse velocity decreases near the upflow zones and increases near the downflow zones.

This work has a good scope for further extension. The governing equation can be taken for an unsteady and nonuniform flow that are not considered here. Apart from that, the model can include effect of sediment presence that will make it applicable for sediment-laden flow.

## 5. Appendix

### 5.1. Numerical solution of the problem

In this section, the numerical solution of the problem using finite difference approximation is discussed. The governing equation (Eq. (2.17)) to be solved can be written as follows:

$$\frac{\partial^2 \tilde{u}}{\partial \tilde{y}^2} + A\frac{\partial^2 \tilde{u}}{\partial \tilde{z}^2} - B\frac{\partial \tilde{u}}{\partial \tilde{y}} + C\frac{\partial \tilde{u}}{\partial \tilde{z}} + D = 0, \tag{5.1}$$

where

$$A = 6\lambda\tilde{z}(1-\tilde{z}), \tag{5.2}$$

$$B = \frac{6}{\kappa}\frac{w_{max}}{\tilde{u}_*}\cos(\pi\tilde{z})\sin(\pi\tilde{y}), \tag{5.3}$$

$$C = 6\lambda(1-2\tilde{z}) + \frac{6}{\kappa}\frac{w_{max}}{\tilde{u}_*}\sin(\pi\tilde{z})\cos(\pi\tilde{y}), \tag{5.4}$$

$$D = \frac{6gSH}{\kappa\tilde{u}_*^2}. \tag{5.5}$$

It can be seen from Eq. (5.1) that the governing equation is an elliptical partial differential equation with variable coefficients. The computational domain is divided into $N$ number of equally spaced grid points with the grid size $\Delta\tilde{y} = \frac{L_y}{N-1}$ in $\tilde{y}$-direction and $M$ number of equally spaced grid points with the grid size $\Delta\tilde{z} = \frac{L_z}{M-1}$ in $\tilde{z}$-direction. $L_y$ and $L_z$ are the lengths of the domain in $\tilde{y}$ and $\tilde{z}$ directions, respectively and the coordinates of the grid points are $\tilde{y}_i = \tilde{y}_1 + i\Delta\tilde{y}$ and $\tilde{z}_j = \tilde{z}_1 + j\Delta\tilde{z}$ in $\tilde{y}$ and $\tilde{z}$ directions, respectively. We discretize Eq. (5.1) at $(i,j)$-th grid point using the standard second order finite difference schemes. Finally, it can be written as:

$$\begin{aligned}(5.6)\qquad &\frac{\tilde{u}_{i+1,j} - 2\tilde{u}_{i,j} + \tilde{u}_{i-1,j}}{\Delta\tilde{y}^2} + A_{i,j}\frac{\tilde{u}_{i,j+1} - 2\tilde{u}_{i,j} + \tilde{u}_{i,j-1}}{\Delta\tilde{z}^2} \\ &\qquad - B_{i,j}\frac{\tilde{u}_{i+1,j} - \tilde{u}_{i-1,j}}{2\Delta\tilde{y}} + C_{i,j}\frac{\tilde{u}_{i,j+1} - \tilde{u}_{i,j-1}}{2\Delta\tilde{z}} + D_{i,j} = 0,\end{aligned}$$

where $i$ and $j$ represent the $i$th and $j$th grid points in $\tilde{y}$ and $\tilde{z}$ directions, respectively and $\tilde{u}_{i,j}$ is the numerical value of $\tilde{u}(\tilde{y},\tilde{z})$ at the point $(i,j)$. The equation Eq. (5.6) can be rearranged as:

$$\begin{aligned}(5.7)\qquad &\left(\frac{A_{i,j}}{\Delta\tilde{z}^2} - \frac{C_{i,j}}{2\Delta\tilde{z}}\right)\tilde{u}_{i,j-1} + \left(\frac{1}{\Delta\tilde{y}^2} + \frac{B_{i,j}}{2\Delta\tilde{y}}\right)\tilde{u}_{i-1,j} - 2\left(\frac{1}{\Delta\tilde{y}^2} + \frac{A_{i,j}}{\Delta\tilde{z}^2}\right)\tilde{u}_{i,j} \\ &\qquad + \left(\frac{1}{\Delta\tilde{y}^2} - \frac{B_{i,j}}{2\Delta\tilde{y}}\right)\tilde{u}_{i+1,j} + \left(\frac{A_{i,j}}{\Delta\tilde{z}^2} + \frac{C_{i,j}}{2\Delta\tilde{z}}\right)\tilde{u}_{i,j+1} = -D_{i,j} \\ &\qquad\qquad \text{for } i = 2,3,\ldots,N-1 \text{ and } j = 2,3,\ldots,M-1,\end{aligned}$$

where

$$\begin{aligned}A_{i,j} &= 6\lambda\tilde{z}_j(1-\tilde{z}_j),\\ B_{i,j} &= \frac{6}{\kappa}\frac{w_{max}}{\tilde{u}_*}\cos(\pi\tilde{z}_j)\sin(\pi\tilde{y}_i),\\ C_{i,j} &= 6\lambda(1-2\tilde{z}_j) + \frac{6}{\kappa}\frac{w_{max}}{\tilde{u}_*}\sin(\pi\tilde{z}_j)\cos(\pi\tilde{y}_j),\\ D_{i,j} &= \frac{6gSH}{\kappa\tilde{u}_*^2}.\end{aligned}$$

The boundary conditions given by Eqs. (2.18)-(2.21) can be discretized as,

$$(5.8)\qquad \tilde{u}_{i,1} = \tilde{u}_a, \quad \tilde{u}_{i,M} = \tilde{u}_s \quad \text{for } i = 1,2,\ldots,N,$$

$$(5.9)\qquad \frac{\tilde{u}_{i,k+1} - \tilde{u}_{i,k-1}}{2\Delta\tilde{z}} = 0 \quad \text{for } i = 1,2,\ldots,N,$$

where $k$ is the grid point at $\tilde{z} = \tilde{z}_d$.

$$\frac{-3\tilde{u}_{1,j} + 4\tilde{u}_{2,j} - \tilde{u}_{3,j}}{2\Delta\tilde{y}} = 0 \quad \text{for } j = 1, 2, \ldots, M \tag{5.10}$$

and

$$\tilde{u}_{N,j} = \tilde{u}_w \quad \text{for } j = 1, 2, \ldots, M, \tag{5.11}$$

respectively.

To avoid the computational difficulty, we transform the double index notation by a single index notation, $n = i + (j-1)N$. Therefore, the discretized equation Eq. (5.7), using the single index notation can be written as follows:

$$\alpha_1\tilde{u}_{n-N} + \alpha_2\tilde{u}_{n-1} + \alpha_3\tilde{u}_n + \alpha_4\tilde{u}_{n+1} + \alpha_5\tilde{u}_{n+N} = -D_n \tag{5.12}$$

for $n = N+2, N+3, \ldots, 2N-1, 2N+2, \ldots, 3N-1, 3N+2, \ldots, (M-2)N-1$, $(M-2)N+2, \ldots, (M-1)N-1$, where

$$\begin{aligned}
\alpha_1 &= \left(\frac{A_n}{\Delta\tilde{z}^2} - \frac{C_n}{2\Delta\tilde{z}}\right), \qquad \alpha_2 = \left(\frac{1}{\Delta\tilde{y}^2} + \frac{B_n}{2\Delta\tilde{y}}\right), \\
\alpha_3 &= -2\left(\frac{1}{\Delta\tilde{y}^2} + \frac{A_n}{\Delta\tilde{z}^2}\right), \quad \alpha_4 = \left(\frac{1}{\Delta\tilde{y}^2} - \frac{B_n}{2\Delta\tilde{y}}\right), \\
\alpha_5 &= \left(\frac{A_n}{\Delta\tilde{z}^2} + \frac{C_n}{2\Delta\tilde{z}}\right).
\end{aligned}$$

The boundary conditions given by Eqs. (5.8)–(5.11) transformed to

$$\begin{aligned}
&\tilde{u}_n = \tilde{u}_a \quad \text{for } n = 1, 2, \ldots, N, \\
&\tilde{u}_n = \tilde{u}_s \quad \text{for } n = (M-1)N+1, (M-1)N+2, \ldots, MN,
\end{aligned} \tag{5.13}$$

$$\tilde{u}_{n+N} - \tilde{u}_{n-N} = 0 \quad \text{for } n = i + (k-1)N, \text{ where } i = 1, 2, \ldots, N, \tag{5.14}$$

$$-3\tilde{u}_n + 4\tilde{u}_{n+1} - \tilde{u}_{n+2} = 0 \quad \text{for } n = 1, 1+N, 1+2N, \ldots, 1+(M-1)N, \tag{5.15}$$

$$\tilde{u}_n = \tilde{u}_w \quad \text{for } n = N, 2N, \ldots, MN, \tag{5.16}$$

respectively. Finally, we have an algebraic system of equations with $MN$ number of unknowns $\tilde{u}_1, \tilde{u}_2, \tilde{u}_3, \ldots, \tilde{u}_{MN}$, defined by

$$P_{(MN\times MN)}U_{(MN\times 1)} = Q_{(MN\times 1)}, \tag{5.17}$$

where

$$P = \begin{pmatrix}
1 & 0 & 0 & . & . & . & . & . & . & . & . & . & . & . & . & . & . & . & 0 & 0 \\
0 & 1 & 0 & . & . & . & . & . & . & . & . & . & . & . & . & . & . & . & 0 & 0 \\
\vdots & \vdots & \vdots & \vdots & \vdots & \vdots & \vdots & \vdots & \vdots & \vdots & \vdots & \vdots & \vdots & \vdots & \vdots & \vdots & \vdots & \vdots & \vdots & \vdots \\
0 & 0 & 0 & . & . & . & 1 & . & . & . & . & . & . & . & . & . & . & . & 0 & 0 \\
0 & 0 & 0 & . & . & . & 0 & -3 & 4 & -1 & . & . & . & . & . & . & . & . & 0 & 0 \\
0 & 0 & 0 & . & \alpha_1 & . & 0 & \alpha_2 & \alpha_3 & \alpha_4 & . & . & \alpha_5 & . & . & . & . & . & 0 & 0 \\
\vdots & \vdots & \vdots & \vdots & \vdots & \vdots & \vdots & \vdots & \vdots & \vdots & \vdots & \vdots & \vdots & \vdots & \vdots & \vdots & \vdots & \vdots & \vdots & \vdots \\
0 & 0 & 0 & . & . & \alpha_1 & . & . & \alpha_2 & \alpha_3 & \alpha_4 & 0 & 0 & . & . & \alpha_5 & . & . & 0 & 0 \\
0 & 0 & 0 & . & . & . & . & . & 0 & 0 & 1 & 0 & 0 & 0 & . & . & . & . & 0 & 0 \\
0 & 0 & 0 & . & . & . & . & . & 0 & 0 & 0 & -3 & 4 & 1 & . & . & . & . & 0 & 0 \\
0 & 0 & 0 & . & . & . & . & . & 0 & 0 & 0 & \alpha_2 & \alpha_3 & \alpha_4 & . & . & . & . & 0 & 0 \\
\vdots & \vdots & \vdots & \vdots & \vdots & \vdots & \vdots & \vdots & \vdots & \vdots & \vdots & \vdots & \vdots & \vdots & \vdots & \vdots & \vdots & \vdots & \vdots & \vdots \\
0 & 0 & 0 & . & . & . & . & . & . & . & . & . & . & . & . & . & . & . & 1 & 0 \\
0 & 0 & 0 & . & . & . & . & . & . & . & . & . & . & . & . & . & . & . & 0 & 1
\end{pmatrix}, \tag{5.18}$$

$$U = \begin{pmatrix} \tilde{u}_1 \\ \tilde{u}_2 \\ \vdots \\ \tilde{u}_N \\ \tilde{u}_{N+1} \\ \tilde{u}_{N+2} \\ \vdots \\ \tilde{u}_{2N-1} \\ \tilde{u}_{2N} \\ \tilde{u}_{2N+1} \\ \tilde{u}_{2N+2} \\ \vdots \\ \tilde{u}_{MN-1} \\ \tilde{u}_{MN} \end{pmatrix} \quad \text{and} \quad Q = \begin{pmatrix} \tilde{u}_a \\ \tilde{u}_a \\ \vdots \\ \tilde{u}_a \\ 0 \\ -D_n \\ \vdots \\ -D_n \\ \tilde{u}_w \\ 0 \\ -D_n \\ \vdots \\ \tilde{u}_s \\ \tilde{u}_s \end{pmatrix}.$$

So, one can easily get the solution by solving Eq. (5.17).

## References


1. T. VON KARMAN, *Mechanische Ähnlichkeit und Turbulenz*, Nachrichten von der Gesellschaft der Wissenschaften zu Göttingen: Mathematisch-physische Klasse, 58–76, 1930.
2. L. PRANDTL, *Recent results of turbulence research*, Technical Memorandum 720, National Advisory Committee for Aeronautics, 1932.

3. D.E. Coles, *The law of the wake in the turbulent boundary layer*, Journal of Fluid Mechanics, **1**, 191–226, 1956.

4. K.V.N. Sarma, P. Lakshminarayana, N.S.L. Rao, *Velocity distribution in smooth rectangular open channels*, Journal of Hydraulic Engineering, **109**, 270–289, 1983.

5. N.L. Coleman, *Velocity profiles with suspended sediment*, Journal of Hydraulic Research, **19**, 3, 211–229, 1981.

6. N.L. Coleman, *Effects of suspended sediment on the open-channel velocity distribution*, Water Resources Research, **22**, 10, 1377–1384, 1986.

7. J. Guo, *Turbulent velocity profile in clear water and sediment-laden flows*, PhD Thesis, Colorado State University, Fort Collins, CO., 1998.

8. K.V.N. Sarma, B.V.R. Prasad, A.K. Sarma, *Detailed study of binary law for open channels*, Journal of Hydraulic Engineering, **126**, 3, 210–214, 2000.

9. S.Q. Yang, S.K. Tan, S.Y. Lim, *Velocity distribution and dip-phenomenon in smooth uniform open channel flows*, Journal of Hydraulic Engineering, **130**, 12, 1179–1186, 2004.

10. J. Guo, P.Y. Julien, *Application of the modified log-wake law in open-channels*, Journal of Applied Fluid Mechanics, **1**, 2, 17–23, 2008.

11. R. Absi, *An ordinary differential equation for velocity distribution and dip-phenomenon in open channel flows*, Journal of Hydraulic Research, **49**, 1, 82–89, 2011.

12. S. Kundu, K. Ghoshal, *An analytical model for velocity distribution and dip-phenomenon in uniform open channel flows*, International Journal of Fluid Mechanics Research, **39**, 5, 381–395, 2012.

13. S.Q. Yang, *Influence of sediment and secondary currents on velocity*, Water Management, **162**, WM5, 299–307, 2009.

14. Z.Q. Wang, N.S. Cheng, *Time-mean structure of secondary flows in open channel with longitudinal bedforms*, Advances in Water Resources, **29**, 11, 1634–1649, 2006.

15. M. Colombini, *Turbulence-driven secondary flows and formation of sand ridges*, Journal of Fluid Mechanics, **254**, 701–719, 1993.

16. S.Q. Yang, S.K. Tan, X.K. Wang, *Mechanism of secondary currents in open channel flows*, Journal of Geophysical Research, **117**, F04014, 2012.

17. D. Daniel Duda, J. Bem, V. Yanovych, P. Pavlicek, V. Uruba, *Secondary flow of second kind in a short channel observed by piv*, European Journal of Mechanics B Fluids, **79**, 444–453, 2020.

18. I. Nezu, A. Tominaga, H. Nakagawa, *Field measurements of secondary currents in straight rivers*, Journal of Hydraulic Engineering, **119**, 5, 598–614, 1993.

19. J.B. Francis, *On the cause of the maximum velocity of water flowing in open channels being below the surface*, Transactions of the American Society of Civil Engineers, **7**, 1, 109–113, 1878.

20. F.P. Stearns, *On the current-meter: together with a reason why the maximum velocity of water flowing in open channel is below the surface*, Transactions of the American Society of Civil Engineers, **12**, 1, 301–338, 1883.

21. C. Murphy, *Accuracy of stream measurements*, Water Supply and Irrigation Paper, **95**, 111–112, 1904.

22. C.H. KEULEGAN, *Laws of turbulence flow in open channels*, Journal of Research of the National Bureau of Standards, **21**, 707–741, 1938.

23. I. NEZU, H. NAKAGAWA, *Cellular secondary currents in straight conduit*, Journal of Hydraulic Engineering, **110**, 173–193, 1984.

24. J. GUO, P.Y. JULIEN, *Turbulent velocity profiles in sediment-laden flows*, Journal of Hydraulic Research, **39**, 1, 11–23, 2001.

25. J. GUO, *Modified log-wake-law for smooth rectangular open channel flow*, Journal of Hydraulic Research, **52**, 1, 121–128, 2013.

26. J. GUO, P.Y. JULIEN, *Modified log-wake law in smooth rectangular open-channels*, [in:] Advances in Hydraulics and Water engineering, I & II, World Scientific, 2002, 87–99.

27. J.Y. LU, *Study on flow velocity distribution of in the yangtze yangtze river riverflow*, Journal of Yangtze River Scientific Research Institute, **1**, 40–49, 1990.

28. H. BONAKDARI, F. LARRARTE, L. LASSABATERE, C. JOANNIS, *Turbulent velocity profile in fully-developed open channel flows*, Environmental Fluid Mechanics, **8**, 1–17, 2008.

29. D.A. LYN, *A similarity approach to open-channel sediment laden flows*, Journal of Fluid Mechanics, **193**, 1, 1–26, 1988.

30. M. MUSTE, V.C. PATEL, *Velocity profiles for particles and liquid in open-channel flow with suspended sediment*, Journal of Hydraulic Engineering, **123**, 9, 742–751, 1997.

31. A. TOMINAGA, I. NEZU, K. EZAKI, H. NAKAGAWA, *Three-dimensional turbulent structure in straight open channel flows*, Journal of Hydraulic Research, **27**, 1, 149–173, 1989.

32. J. LU, Y. ZHOU, Y. ZHU, J. XIA, L. WEI, *Improved formulae of velocity distributions along the vertical and transverse directions in natural rivers with the sidewall effect*, Environmental Fluid Mechanics, **18**, 11, 2018.

33. L. PRANDTL, *Essentials of Fluid Mechanics*, London and Glasgow, Blackie & Son Ltd, 1952.

34. I. NEZU, H. NAKAGAWA, *Turbulence in Open-Channel Flows*, IAHR Monograph, Balkema, Rotterdam, The Netherlands, 1993.

35. L. PRANDTL, *Über die ausgebildete turbulenz*, [in:] 2e Internationaler Kongress der Technischen Mechanik, Verhandlung, Füessli, Zürich, 1926.

36. Z.Q. WANG, N.S. CHENG, *Secondary flows over artificial bed strip*, Advances in Water Resources, **28**, 5, 441–450, 2005.

37. W.H. GRAF, *Hydraulics of Sediment Transport*, McGraw-Hill, New York, USA, 1971.

38. S.Q. YANG, *Turbulent transfer mechanism in sediment-laden flow*, Journal of Geophysical Research, **112**, F01005, 2007.

39. S. IKEDA, *Self forced straight channels in sandy beds*, Journal of the Hydraulic Division, **107**, 4, 389–406, 1981.

40. S. KUNDU, *Prediction of velocity-dip-position at the central section of open channels using entropy theory*, Journal of Applied Fluid Mechanics, **10**, 1, 221–229, 2017.

41. S. KUNDU, K. GHOSHAL, *Effects of secondary current and stratification on suspension concentration in an open channel flow*, Environmental Fluid Mechanics, **14**, 2014.

42. V.A. VANONI, *Experiments on the transportation of suspended sediment by water*, PhD Thesis, California Institute of Technology, Pasadina, California, 1940.

43. X. WANG, N. QIAN, *Turbulence characteristics of sediment-laden flows*, Journal of Hydraulic Engineering, **115**, 6, 781–799, 1989.

44. I. NEZU, W. RODI, *Experimental study on secondary currents in open channel flow*, [in:] 21th IAHR Congress, 115–119, IAHR, Melbourne, 1985.

45. S. KUNDU, *Theoretical study on velocity and suspension concentration in turbulent flow*, PhD Thesis, Indian Institute of Technology Kharagpur, West Bengal, India, 2015.

*Received July 13, 2020; revised version February 10, 2021.*
*Published online April 29, 2021.*